Optical lithography technique for the fabrication of devices from mechanically exfoliated two-dimensional materials

Microelectronic Engineering 154 (2016) 62–68

Contents lists available at ScienceDirect

Microelectronic Engineering

journal homepage: www.elsevier.com/locate/mee

Optical lithography technique for the fabrication of devices from mechanically exfoliated two-dimensional materials

Rui Zhang [a,*], Tao Chen [b], Andrew Bunting [a], Rebecca Cheung [a]

[a] Scottish Microelectronics Centre, Alexander Crum Brown Road, The University of Edinburgh, King's Buildings, Edinburgh EH9 3FF, United Kingdom
[b] State Key Laboratory of Superlattices and Microstructures, Institute of Semiconductors, Chinese Academy of Science, Beijing 100083, China

ARTICLE INFO

Article history:
Received 23 October 2015
Received in revised form 22 January 2016
Accepted 26 January 2016
Available online 26 January 2016

Keywords:
Two-dimensional (2D) electronics
Graphene
Transition metal dichalcogenides (TMDs)
Optical lithography
Reactive ion etching (RIE)

ABSTRACT

Optical lithography technique has been applied to fabricate devices from atomically thin sheets, exfoliated mechanically from kish graphite, bulk MoS_2 and WSe_2. During the fabrication processes, the exfoliated graphene, few-layer MoS_2 and WSe_2 sheets have been patterned into specific shapes as required and metal contacts have been deposited on these two-dimensional sheets to make field effect devices with different structures. The key to the successful implementation of the technique is the appropriate alignment mark design, which can solve the problems of aligning photomasks to the random location, orientation and irregular shape exfoliated two-dimensional sheets on the substrates. Raman characterization performed on the patterned two-dimensional sheets after the fabrication processes shows that little defects have been introduced during fabrication. Field effect has been observed from *I–V* characteristics with the highly doped silicon substrate as the back gate. The extracted field effect hole and electron mobilities of graphene are ~1010 $cm^2\ V^{-1}\ s^{-1}$ and ~3550 $cm^2\ V^{-1}\ s^{-1}$ respectively; and the field effect carrier mobilities of MoS_2 and WSe_2 are ~0.06 $cm^2\ V^{-1}\ s^{-1}$ and ~0.03 $cm^2\ V^{-1}\ s^{-1}$, separately, which are comparable with experimental results of other reports.

1. Introduction

As Moore's Law drives the feature size of silicon transistors to a few nanometers, device operation will reach its limits. Therefore, in order to improve future circuit performance, alternative materials and their associated fabrication technologies need to be developed. In the pursuit of new materials for circuits beyond the silicon era, a great deal of attention has been paid to atomically thin materials such as graphene [1], two-dimensional (2D) hexagonal boron nitride (h-BN) [2] and transition metal dichalcogenides (TMDs) [3–5]. Each of these materials has its own particular physical properties that may play an important role in building high performance devices. For example, graphene is well known for its high carrier mobility [1]. The electron mobility of graphene from kish graphite or highly ordered pyrolytic graphite (HOPG), prepared by mechanical exfoliation, can reach as high as 15,000 $cm^2\ V^{-1}\ s^{-1}$ even at room temperature, outperforming that of silicon by ten times. However, pristine graphene does not have a bandgap, a property that limits its usefulness in certain applications. Some of the TMDs (such as MoS_2 and WSe_2) have attracted much attention for their high on/off current ratio and low off-state current, due to their intrinsic bandgap [3–5], which is complementary to graphene.

Although several large area 2D material synthesis methods, including sublimation of SiC [6] and chemical vapor deposition (CVD) [7–11], have been studied extensively, mechanical exfoliation method can produce 2D flakes with better crystal quality and purity [1,4]. Thus, from the fundamental research, device fabrication, and cost points of view, the mechanical exfoliation technique still prevails. However, other characteristics associated with the exfoliated 2D material sheets are the small size (typically in the micron range), the random distribution and orientation of the sheets on the substrate, as well as the irregular shape of the sheets. Such features of exfoliated sheets pose challenges to device fabrication, mainly in two aspects: patterning of the 2D materials and alignment of the metal contacts to the patterned 2D sheets.

Thus far, most researchers try to avoid patterning the exfoliated 2D materials and fabricate electronic devices on as-exfoliated pristine 2D materials, which make the dimension of the devices hard to control and limits the practical application of such kind of devices. In addition, electron beam lithography (EBL) is the dominant patterning technique in aligning metal contacts to exfoliated 2D sheets to make electronic devices. However, EBL has some drawbacks. For instance, EBL is a serial process and can take a long time to expose the metal contact openings. Moreover, the electron beam irradiation can induce defects in the 2D sheets [12–14], which may degrade the electrical properties of 2D materials [15,16].

* Corresponding author.
E-mail address: rui.zhang@ed.ac.uk (R. Zhang).

http://dx.doi.org/10.1016/j.mee.2016.01.038

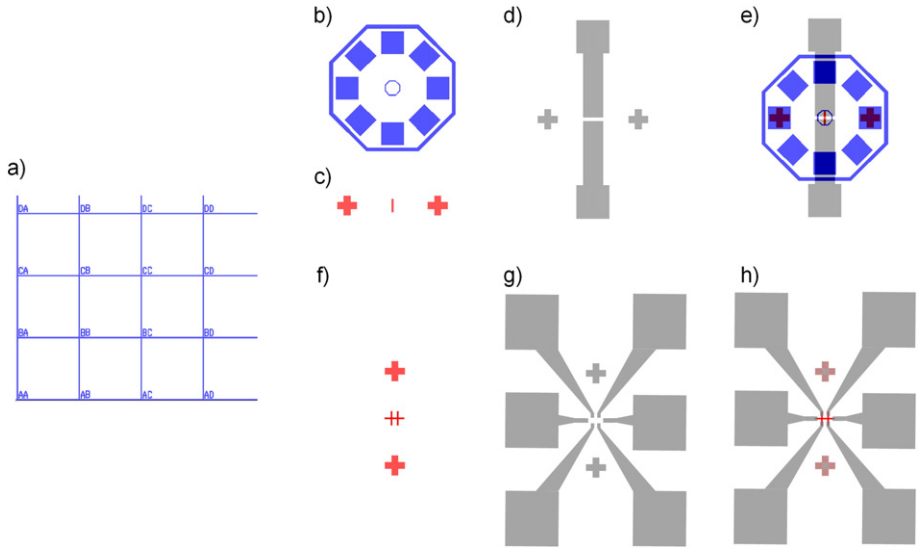

Fig. 1. (a) Grid lines for dividing the substrate into small areas; (b) photomask design for the octagonal-square alignment marks to be patterned around the graphene sheet; photomask design for the channel of graphene (c) and MoS_2/WSe_2 (f) FEDs patterning; photomask design for metal contacts deposition for graphene (d) and MoS_2/WSe_2 (g) FEDs; the whole photomasks set combined together for graphene (e) and MoS_2/WSe_2 (h) FEDs fabrication.

In our work, we report the development of the fabrication of devices from exfoliated 2D sheets using optical lithography. The advantage of employing optical lithography lies in the low cost of the process, the speed of exposure and ease of patterning. The key to the successful implementation of the technique is the alignment mark design. The technique has been applied to fabricate electronic devices designed with a field effect transistor (FET) structure – field effect devices (FEDs) – using pre-patterned graphene, few-layer MoS_2 and WSe_2 sheets as the channels, respectively. To our knowledge, the optical technique reported here is the first of its kind for devices fabricated from exfoliated atomically thin materials.

2. Experiments

Fig. 1 shows the photomask design for graphene, MoS_2 and WSe_2 FEDs fabrication. The photomask in Fig. 1(a) has been employed to divide the substrates into 320 μm × 320 μm grids, so that desired exfoliated 2D sheets can be found under the optical microscope and traced via the labels on the grid lines. In the case of graphene, in order to solve the problem of aligning to the randomly located, oriented, and irregularly shaped exfoliated graphene, alignment marks consisting of four sets of squares (20 μm × 20 μm each) arranged in an octagonal shape around a small octagon in the middle have been designed, as shown in Fig. 1(b). Since any one pair of squares can be used for the alignment, four pairs of squares oriented in different directions can take into account of the random orientation of the exfoliated sheets. Fig. 1(c) and Fig. 1(d) show photomask design of the channel and the electrodes of graphene FED, respectively. Each design has its own alignment marks (crosses), to be aligned onto a pair of squares in the pattern of Fig. 1(b). For the MoS_2 and WSe_2 devices, a different structure has been fabricated with the photomasks in Fig. 1(f, g). Instead of octagonal-square alignment marks in Fig. 1(b), a pair of crosses alignment marks as in Fig. 1(f) has been used to align the pattern in Fig. 1(g) to that in Fig. 1(f). Fig. 1(e, h) shows how the different layers of photomasks are incorporated together.

Firstly, 280 nm of silicon dioxide (SiO_2) has been grown on highly n-doped silicon wafer by thermal wet oxidation, which results in optimal color contrast between the 2D material and substrate [17,18]. The

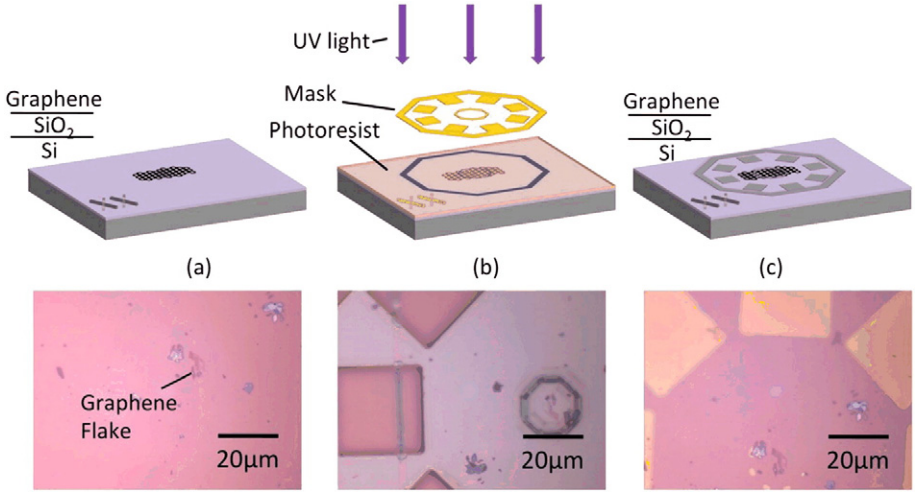

Fig. 2. Patterning of octagonal-square alignment marks around a graphene sheet. The upper part of the figure shows schematic of fabrication processes, while the lower part reveals optical images of the corresponding steps: (a) identification of graphene sheet; (b) transfer the alignment marks on the photoresist with optical lithography technique; (c) etch octagonal-square pattern in SiO_2 by RIE and remove photoresist.

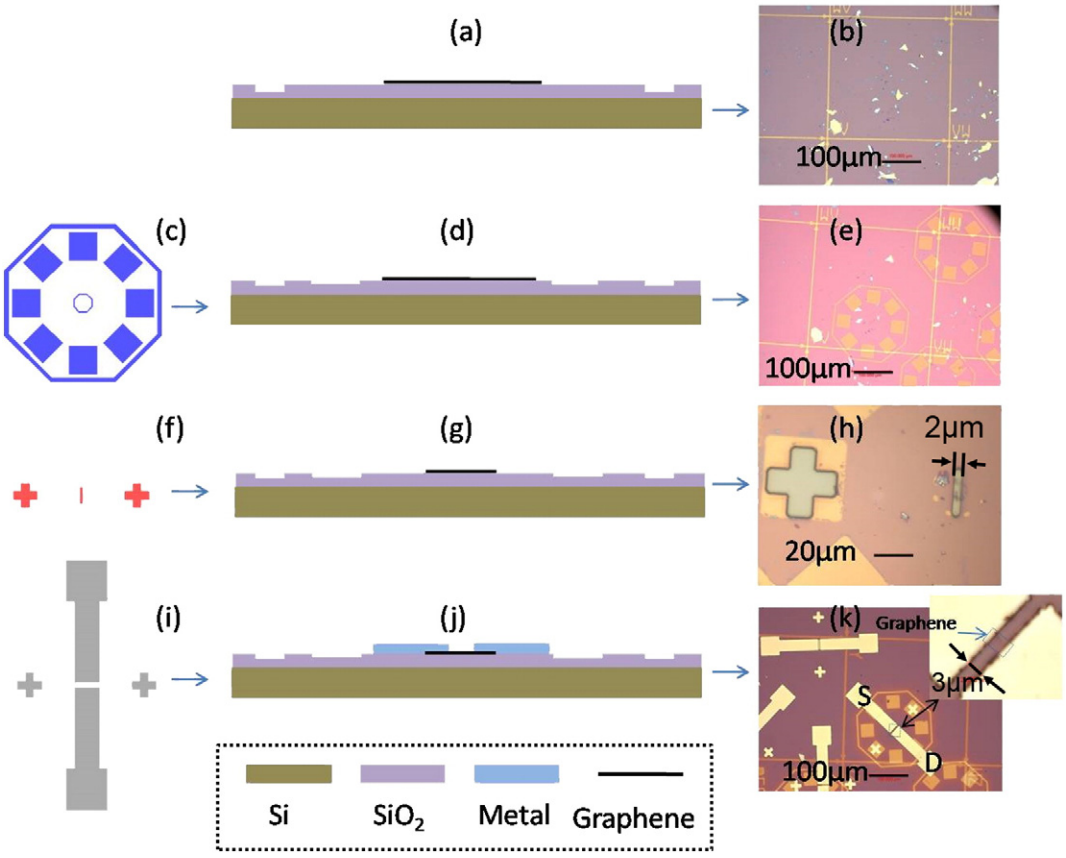

Fig. 3. Fabrication of the graphene FED. The left column shows the pattern of photomasks used in each step; middle column shows the schematic of the fabrication processes; the right column presents the optical images in each corresponding step: (a, b) exfoliate graphene sheets to a labeled substrate; (c–e) align and pattern the octagonal-square alignment marks into SiO_2; (f–h) Align and pattern the graphene channel with O_2 plasma; (i–k) metal contacts fabrication by lift-off of Ti (10 nm)/Al (200 nm) metal layers.

silicon substrate serves as a back gate electrode for the FED, while the SiO_2 serves as the gate dielectric. The wafer then has been diced into 1 cm × 1 cm squares. Afterwards, grid lines (Fig. 1(a)) have been defined on substrates by etching 20 nm deep trenches into the SiO_2 layer with reactive ion etching (RIE). Then, the substrates have been cleaned by sonication in acetone, isopropyl alcohol (IPA), de-ionized (DI) water sequentially and blown dry with N_2 gas. Thereafter, the SiO_2 surface has been treated with O_2 plasma to enhance the bonding between the 2D material and SiO_2 surface [19]. Then, 2D materials have been exfoliated mechanically from the kish graphite (Graphene Supermarket, Inc.), bulk

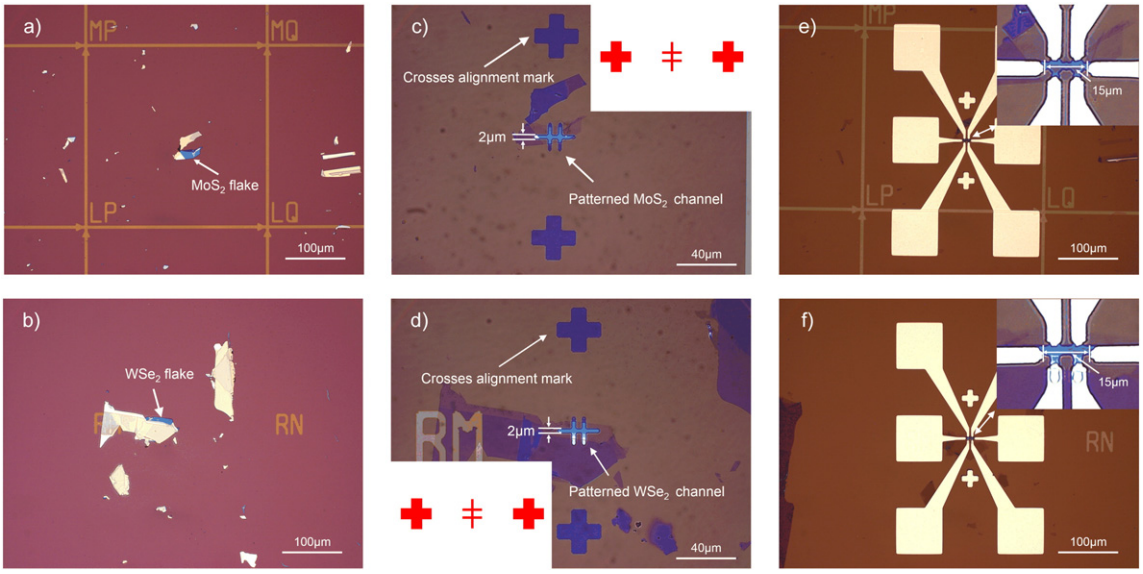

Fig. 4. Optical images of fabrication processes of MoS_2 (first row) and WSe_2 (second row) based FEDs. (a, b) Pristine 2D sheets on labeled substrates; (c, d) 2D sheets have been patterned with CF_4 plasma, leaving alignment marks in the SiO_2 at the same time; the insets show the pattern of photomasks used in this step; (e, f) metal contacts deposition; the insets show the magnified images of the corresponding areas.

MoS_2, and WSe_2 (2D Semiconductors, Inc.) with scotch tapes and transferred onto the substrates. To avoid leaving much tape residual, water soluble tape (3 M water soluble wave solder tape 5414) has been used. After the mechanical exfoliation, the substrates have been soaked in 60 °C DI water to remove the tape residual. Once the graphene and few-layer MoS_2, WSe_2 sheets have been identified by optical microscope according to their color contrast [18,20,21] (Fig. 2(a), Fig. 3(b), and Fig. 4(a, b)), the locations of the 2D sheets on substrates have been recorded by the grid labels they belong to.

Then, for graphene FED fabrication, negative photoresist AZ 2035 has been spun onto the substrate and the octagonal-square alignment marks (Fig. 1(b)) have been defined in SiO_2 layer by optical lithography and RIE of SiO_2 with the center of the octagon pattern in photomask aligned to the graphene sheet with the help of Karl Suss MA/BA8 Mask Aligner, as shown in Fig. 2(b, c) and Fig. 3(c–e). Then, photoresist has been removed with acetone. For MoS_2 and WSe_2 devices fabrication, it is not necessary to etch the octagonal-square alignment marks into SiO_2, since the CF_4 based plasma that is employed to pattern the MoS_2 and WSe_2 sheets also etches into the SiO_2, thus leaving a pair of crosses as alignment marks in the SiO_2 (as shown in Fig. 4(c, d)).

Subsequently, the 2D channels of FEDs have been patterned and defined, as follows (shown in Fig. 3(f–h) and Fig. 4(c, d)). After a layer of positive photoresist SPR 350 has been spin coated on the substrates, for the graphene device, the photomask in Fig. 3(f) has been aligned to the substrate by aligning the crosses to a certain pair of etched octagonal-square alignment marks in SiO_2. After resist exposure and developing, the etch mask with 2 μm width for the channel fabrication has been formed, as indicated in Fig. 3(h). For the MoS_2 and WSe_2 devices, the photomask with a different pattern (as shown in the insets of

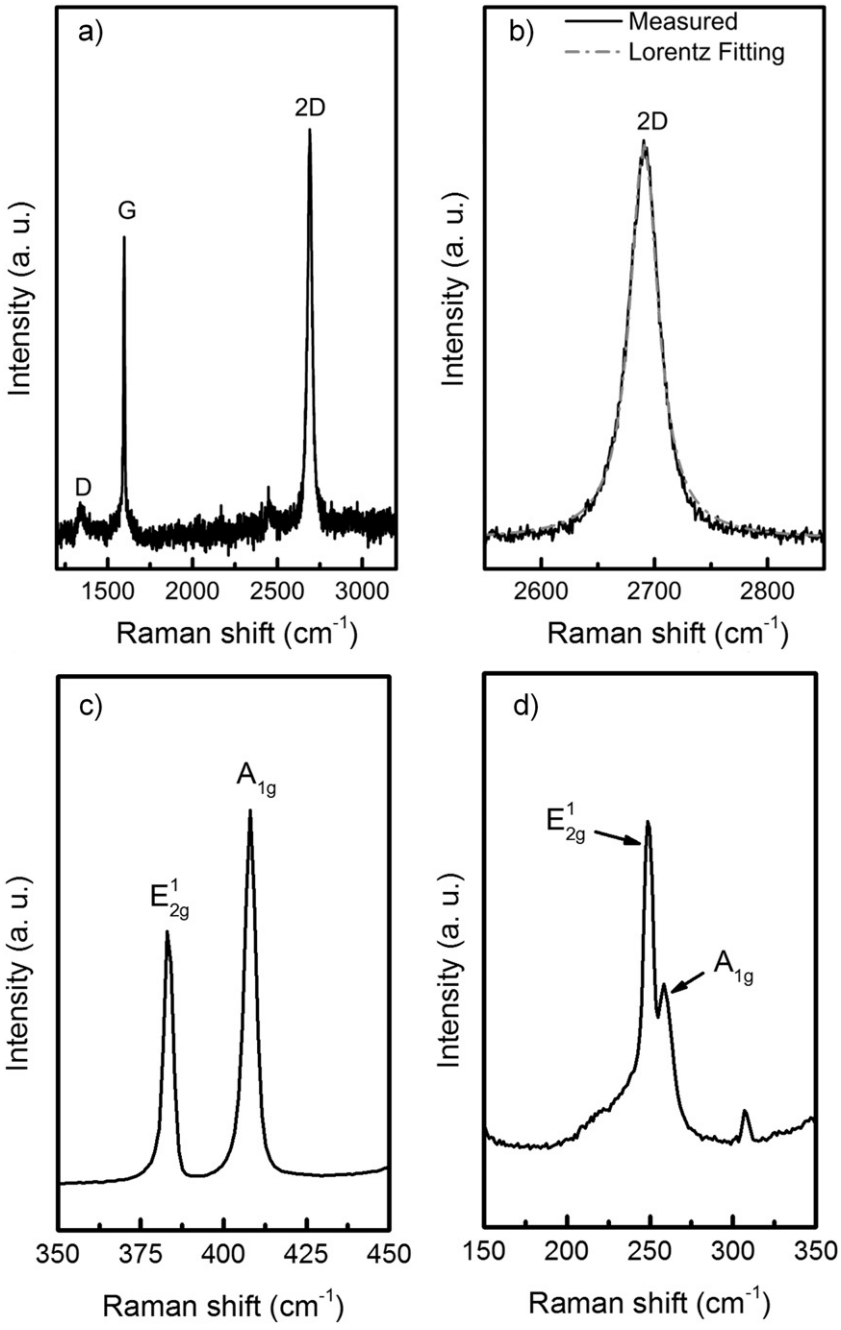

Fig. 5. Raman spectra of the different 2D channels of FEDs: (a, b) Raman spectrum of the graphene in the range of (a) 800–3500 cm^{-1} and (b) 2550–2850 cm^{-1}; (c) Raman spectrum of the few-layer MoS_2 channel in the range of 350–450 cm^{-1}; (d) Raman spectrum of the few-layer WSe_2 channel in the range of 150–350 cm^{-1}.

Fig. 4(c, d)) has been used for photoresist exposure. Then, the graphene sheet has been patterned by O_2 plasma and CF_4 based plasma has been used to pattern MoS_2 and WSe_2 sheets. After removing the photoresist by acetone, the channels of the FEDs have been formed and a pair of crosses alignment marks has been transferred into SiO_2 for the MoS_2 and WSe_2 devices (Fig. 4(c, d)).

For the drain (D) and source (S) contacts fabrication, the regions of contacts with a gap of 3 μm for the graphene device and 15 μm for MoS_2 and WSe_2 devices have been defined on negative photoresist AZ 2035 using photolithography with the help of alignment marks in SiO_2 (octagonal-squares for graphene and a pair of crosses for MoS_2 and WSe_2) formed in previous processes. Afterwards, Ti (10 nm)/Al (200 nm) metal stack has been deposited through E-beam evaporation system and lifted-off in acetone solvent, as shown in Fig. 3(k) and Fig. 4(e, f). After metal deposition, the devices have been annealed in forming gas (N_2/H_2) at 300 °C for 2 h to remove the photoresist residual [22]. Electrical characterization has been carried out using a Keithley 4200-SCS parameter analyzer and Micromanipulator manual probe station at room temperature in air. Raman measurements have been performed on the 2D channels in a confocal Raman spectrometer (inVia Renishaw) with a 100× magnification objective in air ambient environment. The wavelength of the laser is 514 nm. In order to reduce the sample heating effect, the laser power has been kept ~200 μW.

3. Results and discussion

Fig. 5(a, b) shows the Raman spectrum of the graphene channel after the device fabrication. Raman peaks at 1350 cm^{-1}, 1580 cm^{-1} and 2700 cm^{-1}, identified as *D* band, *G* band and *2D* band respectively, have been observed (Fig. 5(a)). A closer look at the *2D* band reveals that the peak is symmetric and can be fitted very well with a single Lorentzian peak (Fig. 5(b)), indicating that the graphene channel is single layer graphene (SLG) [23]. The *D* band around 1350 cm^{-1} is observed to be significantly lower than the *G* band, suggesting that little defects have been induced to the graphene via the fabrication processes. Fig. 5(c) depicts the Raman spectrum of the few-layer MoS_2 channel. The peaks at 382.7 cm^{-1} and 407.6 cm^{-1} are attributed to the in-plane mode (E^1_{2g}) and out-of-plane mode (A_{1g}), respectively [24]. The Raman spectrum of the few-layer WSe_2 channel is displayed in Fig. 5(d). The E^1_{2g} mode (247.8 cm^{-1}) and A_{1g} (257.5 cm^{-1}) mode [25] also have been observed. The weak peak at 307.1 cm^{-1} arises from the interlayer interaction [26]. No other notable Raman peak belonging to other materials (except SiO_2 from the substrate) is found in the Raman spectrum of MoS_2 or WSe_2 channel within the 100–1000 cm^{-1} range (not shown here). The good signal-to-noise (S/N) ratio in Fig. 5(c, d) demonstrates that little damage has been introduced to MoS_2 and WSe_2 sheets from the fabrication processes.

Fig. 6(a–f) shows the transfer characteristics (Fig. 6(a–c)) and output characteristics (Fig. 6(d–f)) of graphene, MoS_2 and WSe_2 based FEDs. Since graphene, MoS_2 and WSe_2 based devices own significantly different electrical properties, due to different electronic band structures of the 2D materials and the barrier heights between the metal contacts and 2D materials, various voltage sweeping ranges have been employed for different devices to exhibit the electrical properties of each device distinctly. The influence of the gate voltage V_{GS} on the drain current I_{DS} with fixed drain voltage V_{DS} for graphene, MoS_2 and WSe_2 devices is depicted in Fig. 6(a–c). For graphene FED (Fig. 6(a)), the drain current I_{DS} decreases as the gate voltage increases from −25 V to 5 V, and starts to increase when the gate voltage surpasses 5 V, showing ambipolar response. The Dirac point, where the drain current is at its minimum and the carriers are depleted most, is seen to occur at around 5 V. When V_{GS} is swept from 5 V to −25 V, a low on/off current ratio of ~1.4 is obtained, due to the absence of bandgap [27]. Compared with graphene, MoS_2 FED exhibits the notable n-type semiconducting behavior (the threshold voltage is about 30 V as shown in Fig. 6(b)), while WSe_2 FED shows p-type behavior with the threshold voltage of −20 V (Fig. 6(c)), which is consistent with the results of Ref. [3] and Ref. [5]. In addition, the corresponding current on/off ratios of the MoS_2 and WSe_2 devices are ~2×10^3 (V_{GS} is swept from 0 V to 60 V) and ~5×10^2 (V_{GS} ranges from 0 V to −70 V), respectively, which are much higher than that of graphene.

With the diffusive transport model proposed by Kim et al. [28], both the hole and electron mobilities of the graphene channel with the dimension of 3 μm in length and 2 μm in width have been extracted to

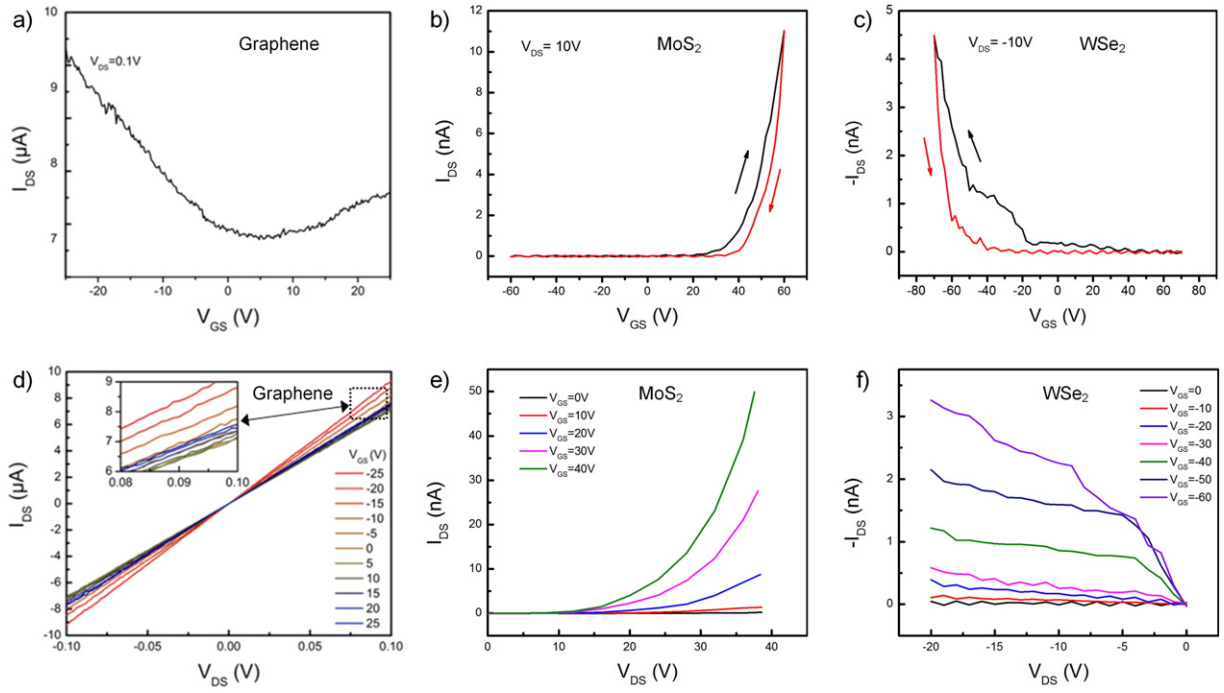

Fig. 6. Drain current (I_{DS}) as a function of gate voltage (V_{GS}) at a fixed drain voltage (V_{DS}) for (a) graphene, (b) MoS_2, and (c) WSe_2 based FEDs; drain current (I_{DS}) as a function of drain voltage (V_{DS}) at different gate voltages (V_{GS}) for (d) graphene, (e) MoS_2, and (f) WSe_2 based FEDs.

be ultrahigh (around 1010 $cm^2 V^{-1} s^{-1}$ and 3550 $cm^2 V^{-1} s^{-1}$ respectively), which correspond well to the reported values of unsuspended graphene [29]. Moreover, the current does not go to zero at the Dirac point, indicating the presence of high intrinsic carrier density in the graphene. The extracted intrinsic carrier density is about 1×10^{12} cm^{-2}. This means that at zero gate voltage, the Fermi energy is below the Dirac point, and the energy-wavevector (E–k) relationship may no longer be linear, which could explain the asymmetry of the I_{DS}–V_{GS} curve observed and the lower hole mobility compared with the deduced electron mobility. For MoS_2 and WSe_2 FEDs, the mobilities have been extracted using the equation $\mu = [dI_{DS}/dV_{GS}] \times [L/(WC_iV_{DS})]$ [30], where $L = 15$ μm is the channel length, $W = 2$ μm is the channel width, and $C_i = 1.23 \times 10^{-4}$ F/m^2 is the capacitance between the channel and back gate per unit area ($\varepsilon_0\varepsilon_r/d$; $\varepsilon_r = 3.9$; $d = 280$ nm). The mobilities of MoS_2 and WSe_2 FED with Ti metal contacts extracted from two point measurements are ~0.06 $cm^2 V^{-1} s^{-1}$ and ~0.03 $cm^2 V^{-1} s^{-1}$, in agreement with the previous reports [3,31,32]. As seen, a mild hysteresis is observed when V_{GS} is swept in reverse directions. The hysteresis can be attributed to charge-trapping effects at the MoS_2 or WSe_2/SiO_2 interface and/or absorbed molecules (moisture and O_2) on the MoS_2 or WSe_2 surface [33,34].

Fig. 6(d–f) shows the dependence of drain current on the drain voltage (I_{DS}–V_{DS}) with different gate voltages V_{GS} for the graphene, MoS_2 and WSe_2 based FEDs. The I_{DS}–V_{DS} curves of graphene FED (Fig. 6(d)) have been observed to be linear when V_{DS} is swept from −0.1 V–0.1 V, suggesting that the graphene device behaves as a resistor. However, for MoS_2 or WSe_2 FEDs, I_{DS}–V_{DS} plots (Fig. 6(e, f)) shows significantly different behavior. When the drain bias V_{DS} of MoS_2 FED is in the range of 0–7 V, the drain current I_{DS} is relatively small and stays almost constant for various gate voltages V_{GS}, as shown in Fig. 6(e). When the drain bias V_{DS} surpasses a certain value and the gate voltage V_{GS} is beyond the threshold voltage, the drain current I_{DS} starts to increase remarkably, which is consistent with the results reported in Ref. [34,35]. The nonlinearity of the I_{DS}–V_{DS} curve could be caused by the Schottky barriers formed between the 2D MoS_2 and Ti layer [36]. On the other hand, for the WSe_2 FED (Fig. 6(f)), the drain current I_{DS} increases at low negative drain voltage and saturates to a certain extent at higher negative drain bias, behaving as a p-type field effect transistor (FET). The characteristic of current saturation in WSe_2 FED plays an important role in the future applications of organic light-emitting diode (OLED) displays [37].

4. Conclusions

Optical lithography technique has been applied for the fabrication of electronic devices from randomly distributed and oriented mechanically exfoliated 2D materials (graphene, few-layer MoS_2 and WSe_2) with random shape. During the development of fabrication processes, patterning of the 2D material channels and the alignment of metal contacts to the patterned 2D channels to make field effect devices have been achieved. The appropriate alignment mark design and implementation are enabling factors in these processes. According to Raman analysis, the 2D materials in the final devices show little defects. From the electrical measurements, the fabricated devices exhibit field effect characteristics, with the extracted mobilities of the 2D channels corresponding to previous reports. The added advantage of the optical technique is that it is fast, cheap and can be applied to the fabrication of devices from any atomically thin exfoliated material.

Acknowledgments

We acknowledge the financial support of UK Engineering and Physical Sciences Research Council (EPSRC) for this work. We would like to thank Andrei Gromov and Oleg Nerushev for help with Raman characterization.

References

[1] K.S. Novoselov, A.K. Geim, S. Morozov, D. Jiang, Y. Zhang, S.A. Dubonos, I. Grigorieva, A. Firsov, Electric field effect in atomically thin carbon films, Science 306 (2004) 666–669.
[2] L. Song, L. Ci, H. Lu, P.B. Sorokin, C. Jin, J. Ni, A.G. Kvashnin, D.G. Kvashnin, J. Lou, B.I. Yakobson, P.M. Ajayan, Large scale growth and characterization of atomic hexagonal boron nitride layers, Nano Lett. 10 (2010) 3209–3215.
[3] B. Radisavljevic, A. Radenovic, J. Brivio, V. Giacometti, A. Kis, Single-layer MoS_2 transistors, Nat. Nanotechnol. 6 (2011) 147–150.
[4] Q.H. Wang, K. Kalantar-Zadeh, A. Kis, J.N. Coleman, M.S. Strano, Electronics and optoelectronics of two-dimensional transition metal dichalcogenides, Nat. Nanotechnol. 7 (2012) 699–712.
[5] H. Fang, S. Chuang, T.C. Chang, K. Takei, T. Takahashi, A. Javey, High-performance single layered WSe_2 p-FETs with chemically doped contacts, Nano Lett. 12 (2012) 3788–3792.
[6] V.Y. Aristov, G. Urbanik, K. Kummer, D.V. Vyalikh, O.V. Molodtsova, A.B. Preobrajenski, A.A. Zakharov, C. Hess, T. Hänke, B. Büchner, I. Vobornik, J. Fujii, G. Panaccione, Y.A. Ossipyan, M. Knupfer, Graphene synthesis on cubic sic/si wafers. perspectives for mass production of graphene-based electronic devices, Nano Lett. 10 (2010) 992–995.
[7] Y. Lee, S. Bae, H. Jang, S. Jang, S.-E. Zhu, S.H. Sim, Y.I. Song, B.H. Hong, J.-H. Ahn, Wafer-scale synthesis and transfer of graphene films, Nano Lett. 10 (2010) 490–493.
[8] J.K. Huang, J. Pu, C.L. Hsu, M.H. Chiu, Z.Y. Juang, Y.H. Chang, W.H. Chang, Y. Iwasa, T. Takenobu, L.J. Li, Large-area synthesis of highly crystalline WSe_2 mono layers and device applications, ACS Nano 8 (2014) 923–930.
[9] Y.C. Lin, W. Zhang, J.K. Huang, K.K. Liu, Y.H. Lee, C.T. Liang, C.W. Chu, L.J. Li, Wafer-scale MoS_2 thin layers prepared by MoO_3 sulfurization, Nanoscale 4 (2012) 6637–6641.
[10] Y.-H. Lee, X.-Q. Zhang, W. Zhang, M.-T. Chang, C.-T. Lin, K.-D. Chang, Y.-C. Yu, J.T.-W. Wang, C.-S. Chang, L.-J. Li, T.-W. Lin, Synthesis of large-area MoS_2 atomic layers with chemical vapor deposition, Adv. Mater. 24 (2012) 2320–2325.
[11] A. Tarasov, P.M. Campbell, M.Y. Tsai, Z.R. Hesabi, J. Feirer, S. Graham, W.J. Ready, E.M. Vogel, Highly uniform trilayer molybdenum disulfide for wafer-scale device fabrication, Adv. Funct. Mater. 24 (2014) 6389–6400.
[12] D. Teweldebrhan, A.A. Balandin, Modification of graphene properties due to electron-beam irradiation, Appl. Phys. Lett. 94 (2009) 013101.
[13] R. Zan, Q.M. Ramasse, R. Jalil, T. Georgiou, U. Bangert, K.S. Novoselov, Control of radiation damage in MoS_2 by graphene encapsulation, ACS Nano 7 (2013) 10167–10174.
[14] A. Garcia, A.M. Raya, M.M. Mariscal, R. Esparza, M. Herrera, S.I. Molina, G. Scavello, P.L. Galindo, M. Jose-Yacaman, A. Ponce, Analysis of electron beam damage of exfoliated MoS_2 sheets and quantitative HAADF-STEM imaging, Ultramicroscopy 146 (2014) 33–38.
[15] I. Childres, L.A. Jauregui, M. Foxe, J. Tian, R. Jalilian, I. Jovanovic, Y.P. Chen, Effect of electron-beam irradiation on graphene field effect devices, Appl. Phys. Lett. 97 (2010) 173109.
[16] C. Durand, X. Zhang, J. Fowlkes, S. Najmaei, J. Lou, A.-P. Li, Defect-mediated transport and electronic irradiation effect in individual domains of CVD-grown monolayer MoS_2, J. Vac. Sci. Technol. B 33 (2015) 02B110.
[17] M.M. Benameur, B. Radisavljevic, J.S. Heron, S. Sahoo, H. Berger, A. Kis, Visibility of dichalcogenide nanolayers, Nanotechnology 22 (2011).
[18] P. Blake, E.W. Hill, A.H. Castro Neto, K.S. Novoselov, D. Jiang, R. Yang, T.J. Booth, A.K. Geim, Making graphene visible, Appl. Phys. Lett. 91 (2007) 063124.
[19] X. Liang, Z. Fu, S.Y. Chou, Graphene transistors fabricated via transfer-printing in device active-areas on large wafer, Nano Lett. 7 (2007) 3840–3844.
[20] H. Li, J. Wu, X. Huang, G. Lu, J. Yang, X. Lu, Q. Xiong, H. Zhang, Rapid and reliable thickness identification of two-dimensional nanosheets using optical microscopy, ACS Nano 7 (2013) 10344–10353.
[21] H. Li, G. Lu, Z. Yin, Q. He, H. Li, Q. Zhang, H. Zhang, Optical identification of single- and few-layer MoS_2 sheets, Small 8 (2012) 682–686.
[22] S.D. Namgung, S. Yang, K. Park, A.-J. Cho, H. Kim, J.-Y. Kwon, Influence of post-annealing on the off current of MoS_2 field-effect transistors, Nanoscale Res. Lett. 10 (2015) 1–6.
[23] A.C. Ferrari, J.C. Meyer, V. Scardaci, C. Casiraghi, M. Lazzeri, F. Mauri, S. Piscanec, D. Jiang, K.S. Novoselov, S. Roth, A.K. Geim, Raman spectrum of graphene and graphene layers, Phys. Rev. Lett. 97 (2006) 187401.
[24] H. Li, Q. Zhang, C.C.R. Yap, B.K. Tay, T.H.T. Edwin, A. Olivier, D. Baillargeat, From bulk to monolayer MoS_2: evolution of Raman scattering, Adv. Funct. Mater. 22 (2012) 1385–1390.
[25] D.G. Mead, J.C. Irwin, Long wavelength optic phonons in WSe_2, Can. J. Phys. 55 (1977) 379–382.
[26] H. Li, G. Lu, Y. Wang, Z. Yin, C. Cong, Q. He, L. Wang, F. Ding, T. Yu, H. Zhang, Mechanical exfoliation and characterization of single- and few-layer nanosheets of WSe_2, TaS_2, and $TaSe_2$, Small 9 (2013) 1974–1981.
[27] F. Schwierz, Graphene transistors, Nat. Nanotechnol. 5 (2010) 487–496.
[28] S. Kim, J. Nah, I. Jo, D. Shahrjerdi, L. Colombo, Z. Yao, E. Tutuc, S.K. Banerjee, Realization of a high mobility dual-gated graphene field-effect transistor with Al_2O_3 dielectric, Appl. Phys. Lett. 94 (2009) 062107.
[29] J. Lee, L. Tao, Y. Hao, R.S. Ruoff, D. Akinwande, Embedded-gate graphene transistors for high-mobility detachable flexible nanoelectronics, Appl. Phys. Lett. 100 (2012) 152104.
[30] R.F. Pierret, Semiconductor Device Fundamentals, Addison-Wesley Reading, MA, 1996.
[31] Y. Zhan, Z. Liu, S. Najmaei, P.M. Ajayan, J. Lou, Large-area vapor-phase growth and characterization of MoS_2 atomic layers on a SiO_2 substrate, Small 8 (2012) 966–971.
[32] W. Liu, J. Kang, D. Sarkar, Y. Khatami, D. Jena, K. Banerjee, Role of metal contacts in designing high-performance monolayer n-type WSe_2 Field effect transistors, Nano Lett. 13 (2013) 1983–1990.

[33] K. Cho, W. Park, J. Park, H. Jeong, J. Jang, T.-Y. Kim, W.-K. Hong, S. Hong, T. Lee, Electric stress-induced threshold voltage instability of multilayer MoS_2 field effect transistors, ACS Nano 7 (2013) 7751–7758.
[34] D.J. Late, B. Liu, H.S.S.R. Matte, V.P. Dravid, C.N.R. Rao, Hysteresis in single-layer MoS_2 field effect transistors, ACS Nano 6 (2012) 5635–5641.
[35] X. Xie, D. Sarkar, W. Liu, J. Kang, O. Marinov, M.J. Deen, K. Banerjee, Low-frequency noise in bilayer MoS_2 transistor, ACS Nano 8 (2014) 5633–5640.
[36] Z. Zhang, K. Yao, Y. Liu, C. Jin, X. Liang, Q. Chen, L.M. Peng, Quantitative analysis of current–voltage characteristics of semiconducting nanowires: decoupling of contact effects, Adv. Funct. Mater. 17 (2007) 2478–2489.
[37] S. Kim, A. Konar, W.S. Hwang, J.H. Lee, J. Lee, J. Yang, C. Jung, H. Kim, J.B. Yoo, J.Y. Choi, Y.W. Jin, S.Y. Lee, D. Jena, W. Choi, K. Kim, High-mobility and low-power thin-film transistors based on multilayer MoS_2 crystals, Nat. Commun. 3 (2012) 1011.